J. Fluid Mech. (2006), *vol.* 552, *pp.* 289–298. © 2006 Cambridge University Press
doi:10.1017/S0022112006008639 Printed in the United Kingdom

A bound on scalar variance for the advection–diffusion equation

By S. C. PLASTING AND W. R. YOUNG

Scripps Institution of Oceanography, University of California, San Diego, CA 92093-0230, USA

(Received 18 October 2005 and in revised form 20 December 2005)

We study the statistics of a passive scalar $T(\boldsymbol{x}, t)$ governed by the advection–diffusion equation with variations in the scalar produced by a steady source. Two important statistical properties of the scalar are the variance, $\sigma^2 \equiv \langle T^2 \rangle$, and the entropy production, $\chi \equiv \kappa \langle |\nabla T|^2 \rangle$. Here $\langle\rangle$ denotes a space–time average and κ is the molecular diffusivity of T. Using variational methods we show that the system must lie above a parabola in the (χ, σ^2)-plane. The location of the bounding parabola depends on the structure of the velocity and the source. To test the bound, we consider a large-scale source and three two-dimensional model velocities: a uniform steady flow; a statistically homogeneous and isotropic flow characterized by an effective diffusivity; a time-periodic model of oscillating convection cells with chaotic Lagrangian trajectories. Analytic solution of the first example shows that the bound is sharp and realizable. Numerical simulation of the other examples shows that the statistics of $T(\boldsymbol{x}, t)$ lie close to the parabolic frontier in the (χ, σ^2)-plane. Moreover in the homogenization limit, in which the largest scale in the velocity field is much less than the scale of the source, the results of the simulation limit to the bounding parabola.

1. Introduction and formulation

The most basic measures of the efficiency of mixing are the mean and variance of the concentration field. Thiffeault, Doering & Gibbon (2005, referred to herein as TDG) have recently posed the problem of bounding the variance of a passive scalar $T(\boldsymbol{x}, t)$ in terms of the molecular diffusivity κ, and gross properties of the advecting velocity field, such as the kinetic energy. These authors consider a scalar contained in a closed domain. The scalar is maintained in a statisitical steady state by applying a source $S(\boldsymbol{x})$ whose domain average is zero. In this circumstance the mean concentration is equal to that of the initial condition, and can be taken to be zero. Thus the scalar variance

$$\sigma^2 \equiv \langle T^2 \rangle \tag{1.1}$$

is the primary descriptor of 'mixedness'. In (1.1) $\langle\rangle$ denotes a volume and time average, defined explicitly below in (1.6). Deriving a useful bound on σ^2 would have important applications in geophysics and engineering.

Passive scalar turbulence is unique in that it parallels many of the properties of true turbulence while being more tractable to mathematical analysis (Shraiman & Siggia 2000). The scalar turbulence problem is therefore an opportunity to test mathematical techniques whose application to true turbulence is speculative. It is in this spirit that we apply variational techniques with parallel applications to the Navier–Stokes equations (e.g. Doering & Constantin 1994; Nicodemus, Grossmann & Holthaus 1997; Doering & Foias 2002).

https://doi.org/10.1017/S0022112006008639 Published online by Cambridge University Press

Consider the forced passive scalar problem

$$T_t + LT = S, \tag{1.2}$$

where L is the advection–diffusion operator

$$L \equiv \boldsymbol{u}\cdot\nabla - \kappa\nabla^2. \tag{1.3}$$

Here, κ is the diffusivity, $S(\boldsymbol{x})$ is a steady prescribed source and $\boldsymbol{u}(\boldsymbol{x}, t)$ is a prescribed velocity with $\nabla\cdot\boldsymbol{u} = 0$. If $\boldsymbol{u}(\boldsymbol{x}, t)$ is a stationary random function of time, while $S(\boldsymbol{x})$ is a determinstic function with zero spatial average, then one expects the scalar $T(\boldsymbol{x}, t)$ to eventually arrive in a statistically steady state.

The domain is either doubly periodic or a closed region with boundary conditions

$$\boldsymbol{u}\cdot\hat{\boldsymbol{n}} = 0, \quad \hat{\boldsymbol{n}}\cdot\nabla T = 0, \tag{1.4}$$

where $\hat{\boldsymbol{n}}$ is the outward normal at the boundary of the domain. With these boundary conditions, the internal source S provides the only production of T.

We use an overbar to denote a time average

$$\bar{F}(\boldsymbol{x}) \equiv \lim_{t\to\infty}\frac{1}{t}\int_0^t F(\boldsymbol{x}, t')\,\mathrm{d}t', \tag{1.5}$$

and angular brackets to denote a space and time average

$$\langle F\rangle \equiv \frac{1}{\Omega}\int \bar{F}(\boldsymbol{x})\,\mathrm{d}\boldsymbol{x}, \tag{1.6}$$

where Ω is the area or volume of the domain. We characterize the statistically steady state using both the variance in (1.1) and the entropy production:

$$\chi \equiv \kappa\langle|\nabla T|^2\rangle. \tag{1.7}$$

The entropy power integral,

$$\chi = \langle TS\rangle, \tag{1.8}$$

is obtained by multiplying (1.2) by T and averaging. The right-hand side of (1.8) is the large-scale production of scalar variance σ^2 by the source S, and the left is the small-scale destruction by diffusion κ. Notice that if the mean field $\bar{T}(\boldsymbol{x})$ is known then the right-hand side of (1.8) can be used to evaluate χ.

Following TDG, a second integral constraint is obtained by forming $\langle C\times$ equation (1.2)$\rangle$, where $C(\boldsymbol{x})$ is an arbitrary 'comparison function'. We take $C(\boldsymbol{x})$ to be time-independent and to satisfy the same no-flux boundary conditions as $T(\boldsymbol{x}, t)$ given in (1.4). The important feature of this restriction on $C(\boldsymbol{x})$ is that the boundary terms generated with integration by parts against $\nabla^2 T$ are all zero. Thus moving all derivatives from T and onto C results in the integral constraint

$$\langle TL^\dagger C - SC\rangle = 0, \tag{1.9}$$

where

$$L^\dagger \equiv -\boldsymbol{u}\cdot\nabla - \kappa\nabla^2 \tag{1.10}$$

is the adjoint of L in (1.3).

2. Bounds connecting χ and σ^2

We now construct a variational problem, built upon the two constraints in (1.8) and (1.9). We seek to bound either the entropy production χ or the variance σ^2, or

https://doi.org/10.1017/S0022112006008639 Published online by Cambridge University Press

to find inequalities connecting these two statistical properties of $T(\boldsymbol{x}, t)$. We begin by writing the variance as

$$\tfrac{1}{2}\sigma^2 = \tfrac{1}{2}\langle T^2\rangle + \alpha(\chi - \langle TS\rangle) + \beta\langle SC - TL^{\dagger}C\rangle. \tag{2.1}$$

In this expression the scalars α and β are loosely recognized as Lagrange multipliers enforcing (1.8) and (1.9). This approach differs from that of TDG by inclusion of the entropy power integral; thus we recover the TDG bound by taking $\alpha = 0$.

Completing the square in T, we rewrite (2.1) as

$$\tfrac{1}{2}\sigma^2 = \tfrac{1}{2}\langle (T - \alpha S + \beta A)^2\rangle + \alpha\chi + \beta\langle SC\rangle - \tfrac{1}{2}\langle(\beta A - \alpha S)^2\rangle, \tag{2.2}$$

where for brevity

$$A \equiv -L^{\dagger}C = \kappa\nabla^2 C + \boldsymbol{u}\cdot\nabla C. \tag{2.3}$$

Dropping the first term on the right of (2.2) we obtain a lower bound on σ^2:

$$\tfrac{1}{2}\sigma^2 \geqslant \alpha\chi + \beta\langle SC\rangle - \tfrac{1}{2}\langle(\beta A - \alpha S)^2\rangle. \tag{2.4}$$

The right-hand side of (2.4) is a convex quadratic function of α and β. Thus one easily maximizes over α and β simultaneously and obtains:

$$\sigma^2 \geqslant \frac{\langle A^2\rangle\chi^2 + 2\langle SA\rangle\langle SC\rangle\chi + \langle SC\rangle^2\langle S^2\rangle}{\langle A^2\rangle\langle S^2\rangle - \langle SA\rangle^2}. \tag{2.5}$$

The integrals on the right are all determined explicitly once the advecting flow field $\boldsymbol{u}(\boldsymbol{x}, t)$, the source function $S(\boldsymbol{x})$ and the comparison function $C(\boldsymbol{x})$ are specified. Minimizing the right-hand side of (2.5) over χ we obtain

$$\sigma^2 \geqslant \frac{\langle A^2\rangle\chi^2 + 2\langle SA\rangle\langle SC\rangle\chi + \langle SC\rangle^2\langle S^2\rangle}{\langle A^2\rangle\langle S^2\rangle - \langle SA\rangle^2} \geqslant \frac{\langle SC\rangle^2}{\langle A^2\rangle}. \tag{2.6}$$

The final expression on the far right of (2.6) is the variance bound of TDG.

The scalar variance is bounded by using any comparison function in (2.6) which satisfies no-flux boundary conditions. However to avoid guessing the $C(\boldsymbol{x})$, one can calculate the optimal comparison function $C_*(\boldsymbol{x})$ by maximizing the right of (2.5) over all C. To perform this variation we introduce the functional

$$\mathscr{F}[A, B, C] \equiv \frac{\mathscr{N}[A, C]}{\mathscr{D}[A]} + \langle B(A + L^{\dagger}C)\rangle, \tag{2.7}$$

where the functional $\mathscr{N}[A, C]$ is the numerator in (2.5) and $\mathscr{D}[A]$ is the denominator. The Lagrange multiplier $B(\boldsymbol{x}, t)$ enforces the definition of $A(\boldsymbol{x}, t)$ in (2.3) as a constraint. The variation $\delta\mathscr{F}/\delta A = 0$ implies that

$$\mathscr{D}B + 2(\chi^2 - \lambda\langle S^2\rangle)A + 2(\chi\langle SC\rangle + \lambda\langle SA\rangle)S = 0. \tag{2.8}$$

The eigenvalue λ above is

$$\lambda = \frac{\mathscr{N}[A_*, C_*]}{\mathscr{D}[A_*]}, \tag{2.9}$$

where $[A_*(\boldsymbol{x}, t), B_*(\boldsymbol{x}, t), C_*(\boldsymbol{x})]$ is the stationary solution. Equation (2.8) determines B in terms of A, C and λ. Setting the variation of $\mathscr{F}[A, B, C]$ with respect to B equal to zero gives (2.3).

To perform the variation of $\mathscr{F}[A, B, C]$ with respect to C, recall that C is time-independent, and that the angular bracket includes both a space and a time average. Therefore variations in $C(\boldsymbol{x})$ will yield a time-averaged equation for the optimal

https://doi.org/10.1017/S0022112006008639 Published online by Cambridge University Press

comparison function. For instance,

$$\frac{\delta}{\delta C}\langle BL^{\dagger}C\rangle = \overline{LB}, \tag{2.10}$$

where the overline is the time average in (1.5). In the course of proving (2.10), one finds that in order for the various boundary terms to vanish, $B(\boldsymbol{x}, t)$ must also satisfy the no-flux condition:

$$\hat{\boldsymbol{n}} \cdot \nabla B = 0; \tag{2.11}$$

this is the 'natural boundary condition' for the variational problem. The final result for the C variation is

$$\mathscr{D}\overline{LB} + 2(\chi\langle SA\rangle + \langle S^2\rangle\langle SC\rangle)S = 0. \tag{2.12}$$

Eliminating $\mathscr{D}B$ between (2.8) and (2.12) one obtains a fourth-order eigenproblem for $C(\boldsymbol{x})$ and λ:

$$(\lambda\langle S^2\rangle - \chi^2)\overline{LL^{\dagger}C} + (\chi S - \lambda\bar{L}S)\langle SL^{\dagger}C\rangle - (\langle S^2\rangle S - \chi\bar{L}S)\langle SC\rangle = 0. \tag{2.13}$$

Given a specific flow field and source, equation (2.13) may be solved to find the optimal comparison function $C_*(\boldsymbol{x})$ and, using $C_*(\boldsymbol{x})$ to calculate the quadratures in (2.5), we obtain an optimized lower bound for the variance. In the following sections we consider three model flows and compare the lower bound in (2.5) with analytic and numerical simulations of the advection–diffusion equation. Solutions of (2.13) will be presented for these model flows.

3. The first example: a uniform flow

Our first example is a simple flow for which both bounds in (2.6) are exact. The domain is doubly periodic, with $0 < (x, y) < 2\pi/k$, and the source is

$$S(\boldsymbol{x}) = \sqrt{2}S_0 \cos ky. \tag{3.1}$$

The velocity is a uniform steady flow, sweeping across the domain: $\boldsymbol{u} = (u, v)$. The steady solution of the advection–diffusion equation is

$$T = \sqrt{2}S_0 \frac{\kappa k^2 \cos ky + kv \sin ky}{(\kappa k^2)^2 + (kv)^2}, \tag{3.2}$$

with variance $\sigma^2 = S_0^2/[(\kappa k^2)^2 + (kv)^2]$ and entropy production $\chi = \kappa k^2 \sigma^2$. It is easy to see that the exact solution of (2.13) is $C = S$ and that both inequalities in (2.6) become equalities. In other words, both bounds are realizable and sharp.

This example is an instructive illustration of difficulties in interpreting the TDG bound as a measure of the mixing efficiency of the velocity field. A uniform steady flow does not amplify tracer gradients and so neither stirs nor mixes in the classic sense (Eckart 1948; Welander 1955). However a uniform steady flow sweeps fluid particles across source regions with both signs. Thus the tracer variance σ^2 is reduced by limiting the action of the source, rather than by amplifying the effect of molecular diffusion. The TDG bound captures this sweeping process and consequently emphasizes the properties of the source (see also Doering & Thiffeault 2005). But the TDG bound takes no account of the entropy power integral (1.8), and therefore does not include gradient amplification. The main advantage of (2.5) is that gradient amplification is captured via χ. The next two examples show that this extra information enhances the bound.

https://doi.org/10.1017/S0022112006008639 Published online by Cambridge University Press

4. The second example: the renewing flow

Next, we illustrate and test the bound in (2.5) using a popular model of a random two-dimensional velocity field (Pierrehumbert 1994; Antonsen *et al.* 1996). Again the domain is doubly periodic, with $0 < (x, y) < 2\pi/k$, and the source is the sinusoid in (3.1). The velocity alternately switches between $v = 0$ and $u = 0$. Specifically, for $n\tau \leqslant t \leqslant n\tau + \tau/2$ the velocity is

$$[u, v] = \sqrt{2}U[\cos(Nky + \phi_x),\ 0], \tag{4.1}$$

and for $n\tau + \tau/2 < t < (n+1)\tau$

$$[u, v] = \sqrt{2}U[0,\ \cos(Nkx + \phi_y)], \tag{4.2}$$

where N is an integer controlling the scale separation between the source and the velocity field, τ is the time over which the velocity switches occur and n is a positive integer. The phases ϕ_x and ϕ_y change every $t = n\tau$ and are uniformly distributed between 0 and 2π. The average squared velocity is $\langle u^2 + v^2 \rangle = U^2$.

The renewing flow is isotropic and homogeneous in the sense that

$$\langle u_i u_j \rangle = \tfrac{1}{2}U^2\delta_{ij}. \tag{4.3}$$

The important consequence of isotropy and homogeneity is that the operator $\overline{LL^\dagger}$ in (2.13) is simply $\overline{LL^\dagger}C = \kappa^2\nabla^4 C - U^2\nabla^2 C$. Moreover, all of the coefficients in the homogeneous equation (2.13) are constant. Consequently, with the single-mode source in (3.1), the solution of (2.13) is simply that C is proportional to $S = \sqrt{2}S_0 \cos ky$. Thus taking $C = S$ is optimal, and (2.6) then gives

$$\frac{\sigma^2}{S_0^2} \geqslant \frac{\chi^2}{S_0^4} + 2\left(\frac{\epsilon\chi}{S_0^2} - \frac{1}{kU}\right)^2 \geqslant \frac{2}{(kU)^2(1 + 2\epsilon^2)}, \tag{4.4}$$

where $\epsilon \equiv \kappa k/U$ is an inverse Péclet number.† In general σ^2 and χ are both unknown so that the inequality in (4.4) constrains these two quantities to lie above a parabola in the (χ, σ^2) parameter plane – see figure 1(*a*).

The simple $C = S$ solution of (2.13) works because: (i) the flow is isotropic and homogeneous; (ii) the source contains only one mode. Doering & Thiffeault (2005) investigate the variance bounds obtained by retaining idealization (i) but relaxing (ii) by considering more complicated sources, e.g. a steady, point release of tracer.

The bound in (4.4) relates the two unknowns χ and σ^2. The result is more informative if one can supply additional information about either χ or σ^2. Thus it is interesting that in the homogenization limit ($N \gg 1$) one can estimate χ. To make this estimate, notice that the single-particle diffusivity of the velocity field in (4.1) and (4.2) is

$$D = \frac{\text{mean squared } x\text{-displacement}}{2 \times \text{time between steps in the } x\text{-direction}} = \frac{U^2\tau}{8}. \tag{4.5}$$

If N is large, so that homogenization applies, then we can make a Reynolds' decomposition, $T = \bar{T}(\boldsymbol{x}) + T'(\boldsymbol{x}, t)$, and compute the mean field $\bar{T}(\boldsymbol{x})$ from $-D\nabla^2\bar{T} = S$. With the sinusoidal source in (3.1):

$$\bar{T}(\boldsymbol{x}) \approx \frac{S(\boldsymbol{x})}{Dk^2} \qquad \text{(provided } N \gg 1\text{)}. \tag{4.6}$$

† When $N = 1$ the Péclet number used by TDG in their section 5 is $\mathrm{P}e = \epsilon^{-1}$.

https://doi.org/10.1017/S0022112006008639 Published online by Cambridge University Press

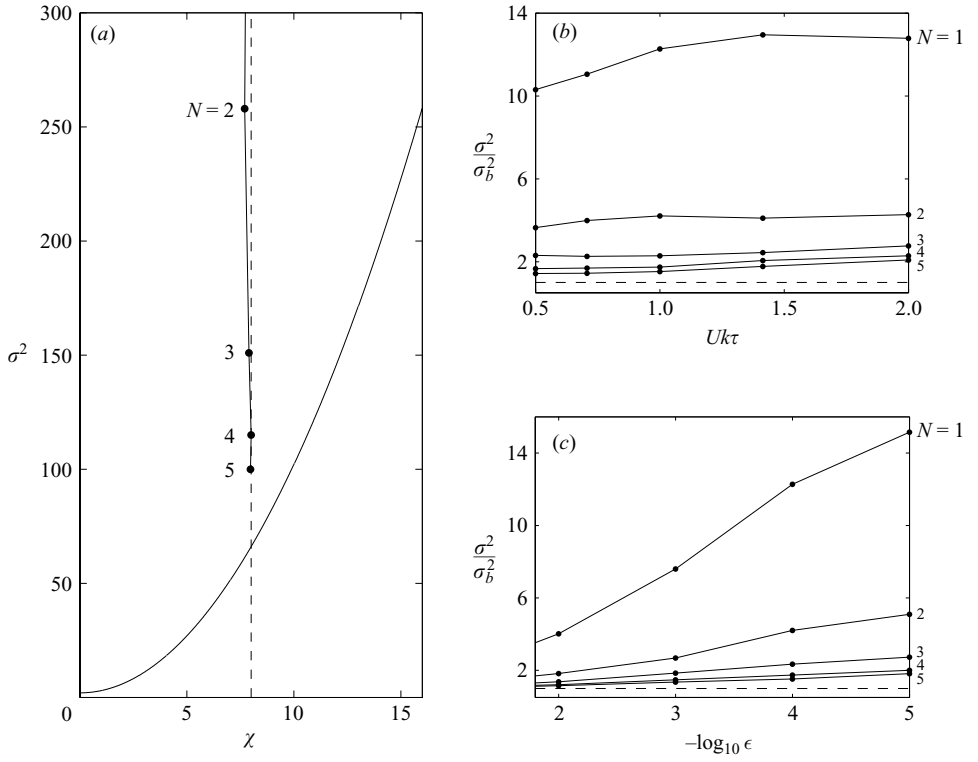


FIGURE 1. Results of numerical simulations of the renewing flow model for $N = 1, \ldots, 5$. Simulations are run up to $t = 500\tau$ at which time reliable statistics may be calculated. (a) Comparison of data points (χ, σ^2) from simulations at fixed $\epsilon = 10^{-4}$ and $Uk\tau = 1$, with the lower bound in equation (4.4). The vertical dashed line is χ obtained from (4.7). The point $N = 1$ is off-scale at $(\chi, \sigma^2) = (8.1, 830)$. ($b, c$) The variance σ^2 is divided by the value of the lower bound evaluated at the simulation value of χ, denoted σ_b^2. In (b) $\epsilon = 10^{-4}$ and both N and $Uk\tau$ are varied. In (c) $Uk\tau = 1$ and both N and ϵ are varied.

Then, using the entropy power integral (1.8), one has

$$\chi = \langle S\bar{T} \rangle \approx \frac{S_0^2}{Dk^2}. \tag{4.7}$$

The numerical results in figure 1(a) show that the mean-field estimate of χ in (4.7) is surprisingly accurate even at $N = 1$. Moreover, as N increases, the points in figure 1 descend vertically along the line $\chi = S_0^2/Dk^2$ and seem to approach the lower bound. We conjecture that the bound is exact in the limit $N \to \infty$.

Figures 1(b) and 1(c) compare simulation data points with the lower bound evaluated at the simulation value of χ. They show again that when the scale separation between source and advecting flow is large the data points are close to the lower bound. In figure 1(b) we see that the velocity strength $Uk\tau$ does not significantly change the ratio of the variance to the lower bound. However, in figure 1(c) there is a much stronger dependence on the Péclet number. In the high diffusion limit the simulation data points approach the bound, as they should, while in the opposite limit of $\epsilon \to 0$ the bound performs less well. Over a moderate range of Péclet number the lower bound performs well with most data points falling well within a decade of the bounding parabola.

https://doi.org/10.1017/S0022112006008639 Published online by Cambridge University Press

5. The third example: oscillating convection cells in a channel

In this section we compare the lower bound on the scalar variance (2.5) with numerical simulations of Solomon & Gollub's (1988) model of oscillating convection cells. The domain is a re-entrant channel with $0 < x < 2\pi/k$. The channel is bounded by walls at $y = 0$ and $y = \pi/m$. The incompressible velocity field is obtained from $(u, v) = (-\psi_y, \psi_x)$, where the model stream function is

$$\psi = \sqrt{2}\psi_0 \sin my \cos[k(x - a\cos\omega t)]. \tag{5.1}$$

As a source we use $S(y) = \sqrt{2}S_0 \cos my$. This example is more complicated than the renewing flow: because of the walls the flow is spatially inhomogeneous and anisotropic. Moreover, chaotic and non-chaotic Lagrangian orbits co-exist, i.e. the phase space is mixed. Reflecting these complications, the eigenvalue problem (2.13) has non-constant coefficients.

An easy bound is obtained by inserting the non-optimal comparison function $C(y) = S$ into (2.5):

$$\frac{\sigma^2}{S_0^2} \geqslant \frac{\chi^2}{S_0^4} + \frac{4}{3}\left(\frac{\chi\epsilon}{S_0^2} - \frac{1}{mk\psi_0}\right)^2, \tag{5.2}$$

where the inverse Péclet number in (5.2) is $\epsilon \equiv (\kappa m)/(\psi_0 k)$.

We improve on (5.2) by solving (2.13) to optimize C. Equation (2.13) is analytically intractable when $C = C(x, y)$, and hence we are less ambitious and consider only one-dimensional comparison functions, $C(y)$. In this case the overlines represents x as well as t averages. For example $\overline{v^2} = k^2\psi_0^2 \sin^2 my$ and the quadratic operator term in (2.13) is

$$\overline{LL^\dagger C} = \partial_y\left[\kappa^2\partial_y^3 - \overline{v^2}\partial_y\right]C. \tag{5.3}$$

Other intermediate results are $\overline{L}S = \kappa m^2 S$ and $\langle SL^\dagger C\rangle = \kappa m^2\langle SC\rangle$. Putting these into (2.13) we have, after some rearrangements to isolate dependence on the eigenvalue λ,

$$\mu\partial_{\hat{y}}\left[\epsilon^2\partial_{\hat{y}}^3 C - \sin^2\hat{y}\,\partial_{\hat{y}}C - 2\epsilon^2\langle C\cos\hat{y}\rangle\sin\hat{y}\right] = \langle C\cos\hat{y}\rangle\cos\hat{y}. \tag{5.4}$$

Above $\hat{y} \equiv my$ and the eigenvalue is

$$\mu \equiv \frac{(\lambda S_0^2 - \chi^2)m^2k^2\psi_0^2}{2(\kappa m^2\chi - S_0^2)^2}. \tag{5.5}$$

Introducing $G \equiv C_{\hat{y}}$, so that $\langle C\cos\hat{y}\rangle = -\langle G\sin\hat{y}\rangle$, and integrating (5.4) once in $\hat{y}$ yields the second-order eigenvalue problem

$$\mu[\epsilon^2 G_{\hat{y}\hat{y}} - \sin^2\hat{y}\,G + 2\epsilon^2\langle G\sin\hat{y}\rangle\sin\hat{y}] + \langle G\sin\hat{y}\rangle\sin\hat{y} = 0. \tag{5.6}$$

The no-flux boundary conditions on C imply that $G(0) = G(\pi) = 0$ and the natural boundary condition in (2.11) requires $G_{\hat{y}\hat{y}}(0) = G_{\hat{y}\hat{y}}(\pi) = 0$. Thus in passing from (5.4) to (5.6) the constant of integration is zero. This is consistent with even symmetry of $G = C_{\hat{y}}$ about $\hat{y} = \pi/2$. These considerations imply that G may be represented as

$$G(y) = \sum_{n=1}^{\infty} G_n \sin[(2n-1)\hat{y}], \tag{5.7}$$

and Galerkin's method may be employed to solve (5.6). It is convenient to impose a normalization constraint, namely $\langle G\sin\hat{y}\rangle = 1$, and then solve the resultant matrix eigenvalue problem numerically. The result of this eigenvalue calculation is shown in

https://doi.org/10.1017/S0022112006008639 Published online by Cambridge University Press

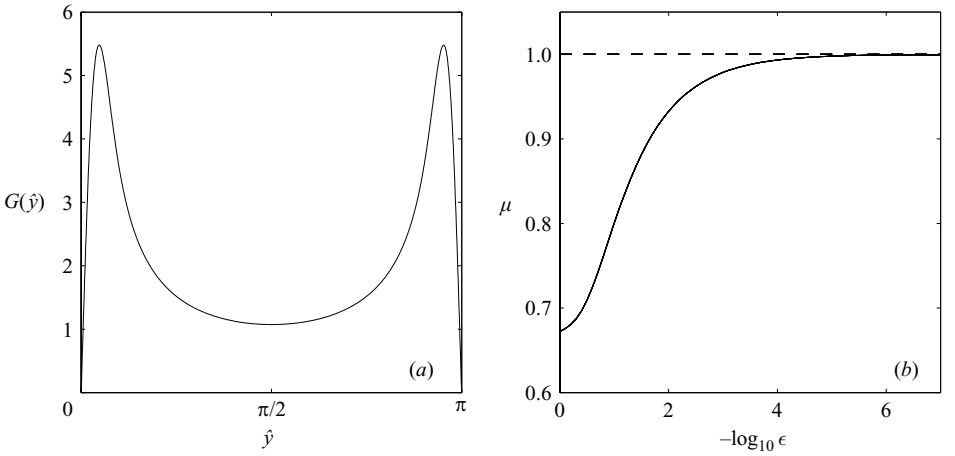


FIGURE 2. Optimal comparison function $C(y)$ for the oscillating convection cell model. (a) The solution $G \equiv C_{\hat{y}}$ to equation (5.6) for $\epsilon \equiv (\kappa m)/(\psi_0 k) = 10^{-2}$. ($b$) The eigenvalue $\mu(\epsilon)$ defined in (5.5) plotted against the logarithm of the Péclet number.

figure 2. The associated bound is

$$\frac{\sigma^2}{S_0^2} \geqslant \frac{\lambda}{S_0^2} = \frac{\chi^2}{S_0^4} + 2\mu(\epsilon)\left(\frac{\chi\epsilon}{S_0^2} - \frac{1}{mk\psi_0}\right)^2, \tag{5.8}$$

where $\mu(\epsilon)$ is the eigenvalue depicted in figure 2(b).

If $\epsilon \equiv (\kappa m)/(\psi_0 k) \ll 1$ then the interior solution of (5.6) is

$$G \approx \frac{\langle G \sin\hat{y}\rangle}{\mu \sin\hat{y}}. \tag{5.9}$$

Boundary layers of thickness $\epsilon^{1/2}$, within which $G = O(\epsilon^{-1/2})$, are required to enforce $G(0) = G(\pi) = 0$. However the integral $\langle G \sin\hat{y}\rangle$ can be evaluated to leading order using only the interior solution (5.9). Thus one finds $\mu(\epsilon) = 1 + O(\epsilon^{1/2})$, which is the asymptote in 2(b). As $\epsilon \to 0$ the prefactor of the squared term in (5.8) is 2, compared to 4/3 in (5.2), which represents a 50 % improvement.

Numerical solutions of the oscillating convection cell model were performed at $\epsilon = 10^{-3}$ for various values of the modulation amplitude a between 0 and 3. The (χ, σ^2) data points for these simulations are shown in figure 3. The maximum mixing (smallest σ^2) is achieved by the steady flow ($a = 0$). The minimum mixing (largest σ^2) is observed at around $a = 2.2$. Snapshots of the scalar field at $a = 2.2$ indicate that there seems to be a transport barrier separating the top half of the channel (where $S(y) < 0$) from the bottom half (where $S(y) > 0$). The inset in figure 3 shows that the simulations are mostly within a decade of the lower bound.

6. Discussion and conclusions

Using variational methods we have shown that the scalar variance σ^2 is bounded from below by a quadratic function of the entropy production χ. This inequality restricts statistics of solutions to lie above a parabola in the (χ, σ^2)-plane.

The variational problem utilizes a time-independent comparison function $C(\boldsymbol{x})$ and imposes the time average of the passive scalar equation (1.2). In the case of the

https://doi.org/10.1017/S0022112006008639 Published online by Cambridge University Press

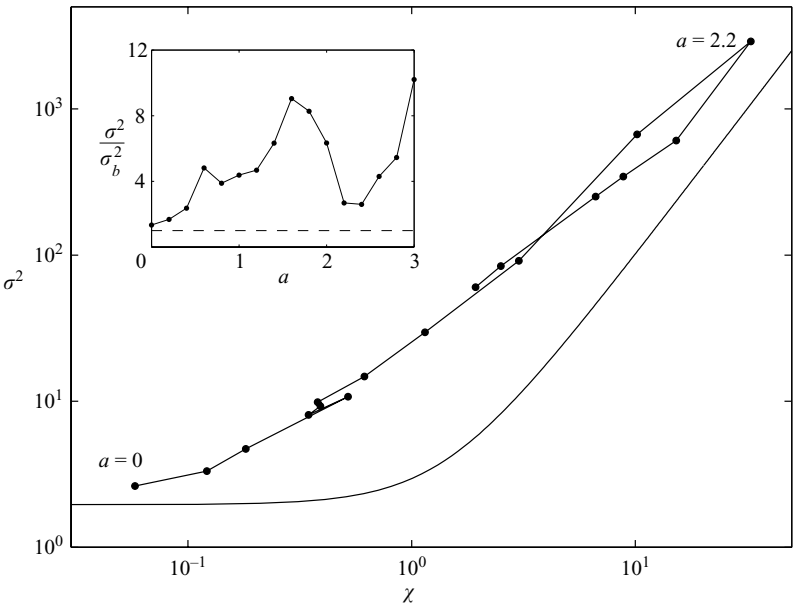


FIGURE 3. Results of numerical simulations of the oscillating convection cell model. The data points are obtained from simulations with $\epsilon = 10^{-3}$ and $\omega = k = m = 1$. The smooth solid curve is the lower bound (5.8) with $\mu(10^{-3}) = 0.979$. The modulation amplitude, a, varies between 0 and 3. Because of the range of numerical values the axes are logarithmic. The inset shows the scalar variance, divided by the lower bound evaluated at the simulation value of χ, plotted against the modulation amplitude.

renewing flow model, with large-scale monochromatic source and doubly periodic boundaries, the optimal choice for C is simply the source function itself. However, for the oscillating convection cell model the optimal equations for the comparison function while being too complicated to solve in two dimensions, give rise to a boundary layered comparison function when solved with a simplified comparison function of a single coordinate $C(y)$.

The closeness of statistics obtained from numerical simulations to the bounding parabola is gratifying. In fact, most data points fall within a decade of the lower-bound parabola. For the renewing flow model we postulate that the lower bound is achieved as the scale separation between the source function and velocity field, namely N in (4.1) and (4.2), becomes large. An interesting question is whether this sharpness extends to situations where the source is not monochromatic and the advecting fields are more complex.

Of key interest is the result that isotropic and homogeneous velocity fields lead to simple solutions of the optimization equation (2.13). How bounding results extend to more diverse source functions, such as a steady point release of scalar, under this class of flow field is therefore an important ongoing area of research (Doering & Thiffeault 2005).

We thank C. R. Doering and J.-L. Thiffeault for many helpful suggestions. This work was supported by the National Science Foundation under the Collaborations in Mathematical Geosciences initiative (grant number ATM0222109 and ATM0222104).

https://doi.org/10.1017/S0022112006008639 Published online by Cambridge University Press

REFERENCES

Antonsen, T. M., Fan, Z., Ott, E. & Garcia-Lopez, E. 1996 The role of chaotic orbits in the determination of power spectra of passive scalars. *Phys. Fluids* **8**, 3094–3104.

Doering, C. R. & Constantin, P. 1994 Variational bounds on energy dissipation in incompressible flows: Shear flow. *Phys. Rev.* E **49**, 4087–4099.

Doering, C. R. & Foias, C. 2002 Energy dissipation in body-forced turbulence. *J. Fluid Mech.* **467**, 289–306.

Doering, C. R. & Thiffeault, J.-L. 2005 Multiscale mixing efficiency for rough sources. *Phys. Rev. Lett.* (submitted).

Eckart, C. 1948 An analysis of the stirring and mixing processes in incompressible fluids. *J. Mar. Res.* **7**, 265–275.

Nicodemus, R., Grossmann, S. & Holthaus, M. 1997 Improved variational principle for bounds on energy dissipation in turbulent shear flow. *Physica* D **101**, 178–190.

Pierrehumbert, R. T. 1994. Tracer microstructure in the large-eddy dominated regime. *Chaos, Solitons Fractals* **4**, 1091–1110.

Shraiman, B. I. & Siggia, E. D. 2000 Scalar turbulence. *Nature* **405**, 639–646.

Solomon, T. H. & Gollub, J. P. 1988 Chaotic particle-transport in time-dependent Rayleigh–Bénard convection. *Phys. Rev.* A **38**, 6280–6286.

Thiffeault, J.-L., Doering, C. R. & Gibbon, J. D. 2004 A bound on mixing efficiency for the advection-diffusion equation. *J. Fluid Mech.* **521**, 105–114 (referred to herein as TDG).

Welander, P. 1955 Studies on the general development of motion in a two-dimensional, ideal fluid. *Tellus* **7**, 141–156.

https://doi.org/10.1017/S0022112006008639 Published online by Cambridge University Press